Hindawi Publishing Corporation
International Journal of Photoenergy
Volume 2014, Article ID 683654, 6 pages
http://dx.doi.org/10.1155/2014/683654

Research Article

Effective Passivation of Large Area Black Silicon Solar Cells by SiO_2/SiN_x:H Stacks

Zengchao Zhao, Bingye Zhang, Ping Li, Wan Guo, and Aimin Liu

School of Physics and Optoelectronic Technology, Dalian University of Technology, Dalian 116023, China

Correspondence should be addressed to Aimin Liu; aiminl@dlut.edu.cn

Received 30 December 2013; Accepted 3 February 2014; Published 6 March 2014

Academic Editor: Tao Xu

The performance of black silicon solar cells with various passivation films was characterized. Large area ($156 \times 156\ mm^2$) black silicon was prepared by silver-nanoparticle-assisted etching on pyramidal silicon wafer. The conversion efficiency of black silicon solar cell without passivation is 13.8%. For the SiO_2 and SiN_x:H passivation, the conversion efficiency of black silicon solar cells increases to 16.1% and 16.5%, respectively. Compared to the single film of surface passivation of black silicon solar cells, the SiO_2/SiN_x:H stacks exhibit the highest efficiency of 17.1%. The investigation of internal quantum efficiency (IQE) suggests that the SiO_2/SiN_x:H stacks films decrease the Auger recombination through reducing the surface doping concentration and surface state density of the Si/SiO_2 interface, and SiN_x:H layer suppresses the Shockley-Read-Hall (SRH) recombination in the black silicon solar cell, which yields the best electrical performance of b-Si solar cells.

1. Introduction

For crystalline silicon solar cells, improving the conversation efficiency is one of the most important and challenging problems. It is well known that antireflection films on solar cells work effectively only at a limited range and for special angles of incidence light. In order to reduce the light loss, the texturing of front surfaces on crystalline silicon solar cells is mostly performed for improvement of the cell efficiency, by means of its antireflection properties and light trapping. Recently the black silicon (b-Si) has attracted much attention due to its excellent antireflection (AR) property [1, 2]. Several b-Si etching methods have been developed, including reactive ion etching [3], plasma immersion ion implantation etching [4, 5], metal nanoparticle assisted etching [6–8], and laser-induced etching [9]. Among these methods, the metal nanoparticle assisted etching is demonstrated to be a mainstream fabrication technique for texturing large area Si wafer due to the low cost and easy preparation for large area solar cells. Great efforts have been made to achieve more efficient b-Si solar cells, but despite the progress, the conversion efficiency is not significantly improved as expected. The dismal performance of b-Si solar cells is mainly due to the enhanced surface recombination and Auger recombination in wafer-based nanostructured silicon solar cells [10]. Therefore, passivation plays an important role to depress the surface recombination in fabrication of high efficiency b-Si solar cells. Recently, the depressive passivation of b-Si becomes a bottleneck, which restricted the development of b-Si solar cells. Thus, choosing appropriate passivation thin films is proven to be very important to develop the performance of silicon solar cells. Great efforts have been made to obtain high efficient Si solar cells by using various passivation materials, such as silicon dioxide (SiO_2), silicon nitride (SiN_x:H), and aluminum oxide (Al_2O_3) [4, 11, 12]. Among these passivation materials, thermal SiO_2 is one of the obvious candidates to realize the above purpose due to simple technique and low cost, given the low density of interface states. In addition, hydrogenated silicon nitride is one of the most significant technological evolutions that have taken place in the solar cell industry, due to its ability to act simultaneously as antireflective film as well as a source of hydrogen for surface and bulk defect passivation. Although several investigations have been carried out to obtain high efficient b-Si solar cells, the results are also depressing, which requires more investigations to clarify the passivation

mechanism and break through the bottleneck of b-Si solar cells.

In our paper, the b-Si wafers with binary structure surface based on silver nanoparticle assisted etching are fabricated. The binary structure textured surface with silicon nanowires (SiNWs) on the pyramidal structure has lower area and better short wavelength response than the conventional b-Si surface with nanostructure on the planar silicon surface [11]. To depress the surface recombination of b-Si solar cells, three kinds of passivation film are prepared on the b-Si solar cells, SiO_2, SiN_x:H, and a bi-layer passivation schemes of SiO_2/SiN_x:H stacks film, which combines a thin thermal oxide with a low density of interface traps and a thick SiN_x film, acting as a source of hydrogen during further solar cell processing. The structural, optical, and electrical properties with various passivation films were investigated.

2. Materials and Methods

We perform alkaline etch and then the two-step black etch to create binary structure textured surface. Four P-type ⟨100⟩ unpolished monocrystalline silicon wafers with resistivity of 1–3 Ω·cm, area of 156 mm × 156 mm, and thickness of 250 ± 20 μm were used in the experiment. Before etching silicon, the wafers were immersed in 10% HF for 1 min to remove any native oxide and rinsed in deionized water. The cleaned wafers were textured in KOH (2 wt%) solution and IPA at 80°C for 30 min to form pyramidal structures. The black etch can be summarized in the following two steps. Firstly, a thin silver nanoparticle layer was deposited on the textured silicon surface from solution I. Subsequently, the Ag nanoparticle covered Si wafers were immersed into mixture solution II at room temperature to fabricate nanowires on the pyramidal structure. To remove the Ag layer completely, the as-prepared samples were treated in a conventional Ag etchant solution consisting of $NH_4OH : H_2O_2 : DI$ in the ratio of 1 : 1 : 5 by volume. Subsequently, the samples were rinsed with DI water and dried with pure N_2.

Solution I and Solution II are the following solutions, respectively:

Solution I (for metallizing): 0.01 mol/L $AgNO_3$ and 4% HF,

Solution II (for etching): 4% HF and 1.2% H_2O_2.

For the solar cell fabrication, n-type emitter was generated by doping the p-type silicon with phosphorus oxychloride ($POCl_3$) diffusion at the temperature 845°C forming a p-n junction underlying the nanowires. The emitter sheet resistance is around 55Ω/□. A diluted HF solution was used to remove the phosphor silicate glass (PSG) layer and rinsed in deionized water. Three of b-Si wafers were passivated with SiO_2, silicon nitride SiN_x:H, and SiO_2/SiN_x:H stacks, respectively. One keeps unpassivated surface. SiO_2 was thermally grown on the samples surface at 850°C for 15 min. After edge isolation, the SiN_x:H was deposited by plasma enhanced chemical vapor deposition (PECVD). Then the back and front sides were screen printed with silver-aluminum, aluminum, and silver pastes, followed by baking

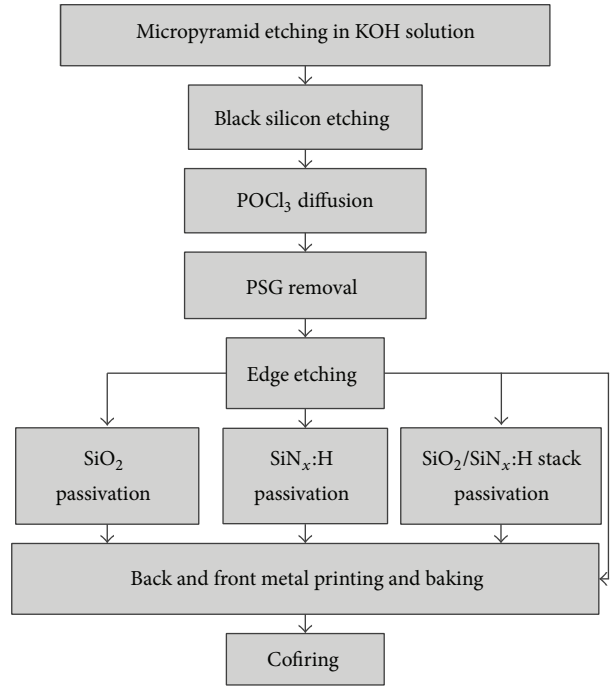

Figure 1: Fabrication process flow chart of the b-Si solar cells.

the pastes on the printed wafers. Finally, dried wafers were cofired in furnace to achieve ohmic contact at both of the front and rear side. The complete process flow chart was shown in Figure 1.

The morphology of the silicon nanowire structure was observed by field effect scanning electron microscope (FESEM) on Hitachi S-4800. Optical reflectance of the b-Si wafers was detected using a spectrophotometer with an integrating sphere. The internal quantum efficiency (IQE) of b-Si solar cells was measured by quantum efficiency measuring system. The doping concentration of diffused b-Si wafers was measured by electrochemical capacitance voltage (ECV) measurement on CVP 21. The electrical performances of b-Si solar cells were characterized using illuminated current-voltage under one sun global spectrum of AM1.5.

3. Results and Discussion

Figure 2 exhibits the images of top view and cross-sectional view on the surfaces of pyramidal textured silicon wafer and typical binary structure textured b-Si wafer. From Figure 2, it is shown that the SiNWs structures have been formed on the pyramidal structure surface. The nanowires which form along the [001] crystal axis are not vertical on the pyramid facets ([111] orientation), as shown in Figure 2(b). The average length and diameter of the nanowires are about 250 nm and 50 nm, respectively. The formation mechanism of SiNWs arrays can be well understood as being a self-assembled Ag-induced selective etching process; catalyst Ag takes an important role in the experiment. The whole reaction was divided into two parts:

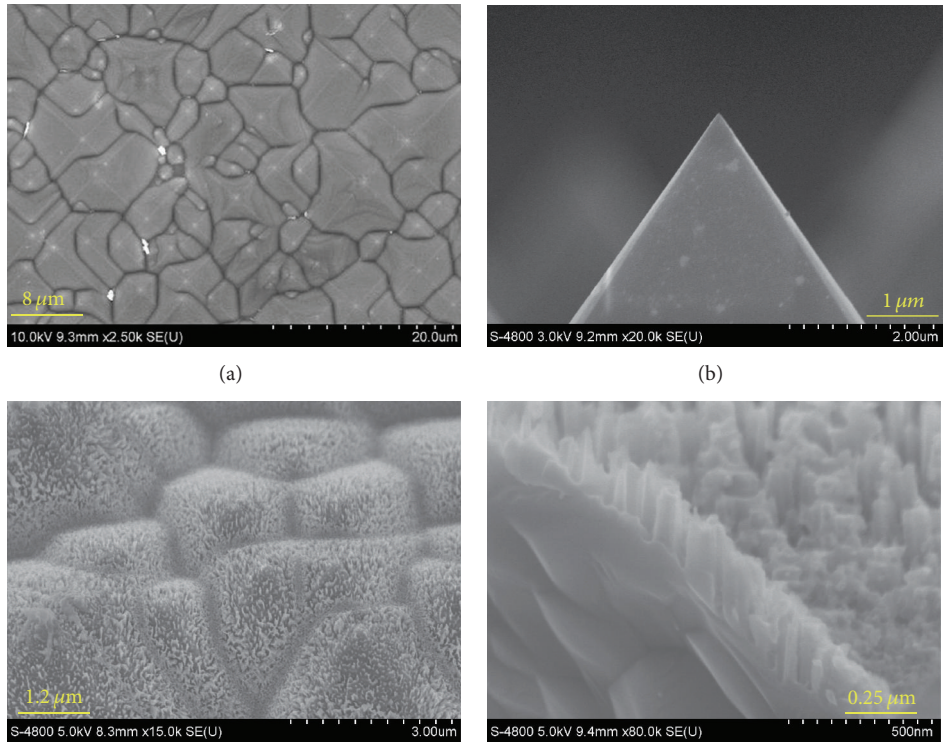

FIGURE 2: SEM images of top view (a) and cross-sectional view (b) of pyramidal textured Si. SEM images of top view (c) and cross-sectional view (d) of as-etched binary structure textured b-Si.

cathode and anode reactions, which are described as follows [13]:

cathode reaction (at silver):

$$\begin{aligned} H_2O_2 + 2H^+ &\longrightarrow 2H_2O + 2h^+ \\ 2H^+ + 2e^- &\longrightarrow H_2\uparrow \end{aligned} \quad (1)$$

anode reaction:

$$\begin{aligned} Si + 4h^+ + 4HF &\longrightarrow SiF_4 + 4H^+ \\ SiF_4 + 2HF &\longrightarrow H_2SiF_6 + 4H^+ \end{aligned} \quad (2)$$

over reaction:

$$Si + H_2O_2 + 6HF \longrightarrow 2H_2O + H_2SiF_6 + H_2\uparrow \quad (3)$$

Figure 3 presents the reflectance of b-Si wafers and pyramidal structure wafer measured over the wavelength from 350 to 1000 nm. A remarkable decrease of reflectance in b-Si wafer was observed. The spectrum-weighted average reflectance (R_{ave}) can be defined as [14]

$$R_{ave} = \frac{\int_{350}^{1000} R(\lambda)\, N(\lambda)\, d\lambda}{\int_{350}^{1000} N(\lambda)\, d\lambda}, \quad (4)$$

where $R(\lambda)$ is the total reflectance and $N(\lambda)$ is the solar flux under AM 1.5 standard conditions. By calculation, the R_{ave} of the pyramidal structure wafer is 11.24%, while that of the

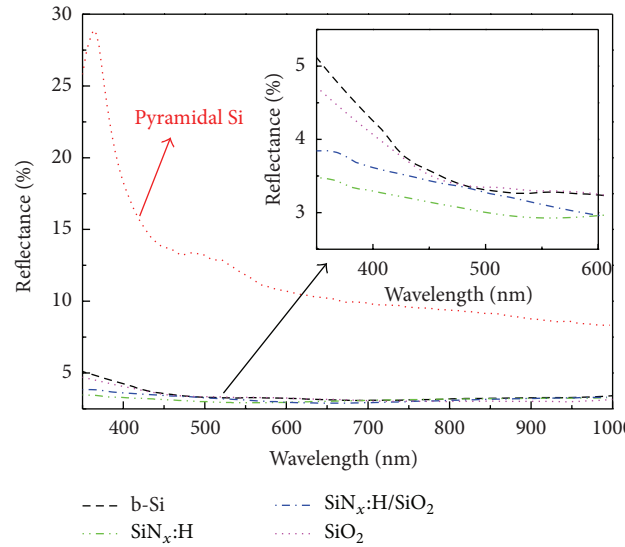

FIGURE 3: Reflectance as function of wavelength of b-Si and pyramidal Si. Insert shows the reflectance of b-Si and b-Si with different passivation films including SiO_2, SiN_x:H, and SiO_2/SiN_x:H, respectively.

b-Si, b-Si with SiO_2, SiN_x:H, and SiO_2/SiN_x:H films is 3.42%, 3.29%, 3.08%, and 3.20%, respectively. A remarkable decrease of reflectance is observed for the SiNWs surface. The antireflection property of SiNWs array surface can be attributed to the morphology of SiNWs which is resembled with subwavelength-structure surface (SWS) [15]. In addition,

Table 1: The electrical properties of the black silicon solar cells with different passivation films.

#	Passivation films	V_{oc} (V)	I_{sc} (A)	FF (%)	η (%)
S1	No passivation	0.598	7.470	73.71	13.8
S2	SiO_2	0.616	8.027	77.31	16.1
S3	SiN_x:H	0.615	8.409	76.04	16.5
S4	SiO_2/SiN_x:H	0.623	8.412	77.81	17.1

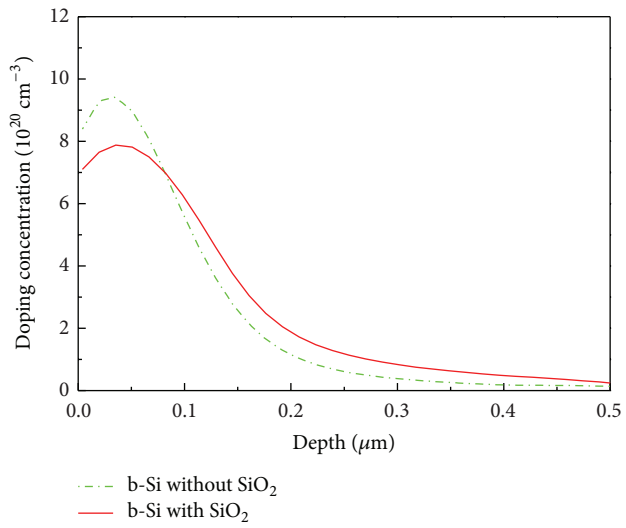

Figure 4: Doping profile for the diffused emitter of b-Si solar cells with and without SiO_2 passivation film by ECV.

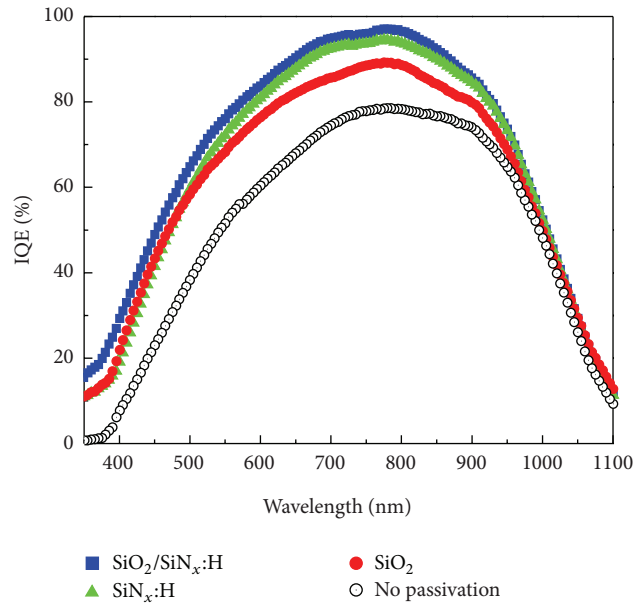

Figure 5: Internal quantum efficiency (IQE) spectra of the b-Si solar cell and b-Si solar cells with SiO_2, SiN_x:H, and SiO_2/SiN_x:H stacks passivation films.

because of unique morphology, there is porosity variation from top to bottom in the nanowire arrays which may cause a gradient in the refractive index with depth and, therefore, SiNWs arrays may give effectively the same antireflection properties as obtained in multilayer antireflection film.

The illuminated current-voltage (I–V) characteristics of the b-Si solar cells with passivation of SiO_2, SiN_x:H, SiO_2/SiN_x:H stacks were measured and the electrical properties were listed in Table 1. It can be found that the conversion efficiency (η) of the solar cell without surface passivation (denoted as S1) is 13.8%, with open circuit voltage (V_{oc}) of 0.598 V, short circuit current (I_{sc}) of 7.470 A, and fill factor (FF) of 73.1%, as shown in Table 1. The low V_{oc} and I_{sc} result from the excess carrier recombination at the nanostructured surface of b-Si solar cell due to the surface recombination. The efficiency of the b-Si solar cell with SiO_2 film (denoted as S2) increases to 16.1%, with the V_{oc} of 0.616 V, I_{sc} of 8.027 A, and FF of 77.31%. For the b-Si solar cell with SiN_x:H film (denoted as S3) of 70 nm thickness, it can be found that the electrical performance increases to η = 16.5%. To further improve the quality of passivation, the SiO_2/SiN_x:H stacks passivation film (denoted as S4) was fabricated on b-Si solar cells. The best electrical performance of b-Si cells appears with η of 17.1%, I_{sc} of 8.412 A, V_{oc} of 0.623 V, and FF of 77.81%.

In order to investigate the passivation effects of SiO_2 layer, doping profile of diffused emitter was measured by ECV, as shown in Figure 4. The surface doping concentration of b-Si solar cells was 9.6×10^{20} cm^{-3}, which means the Auger recombination associated with heavily doped emitter shows a significant influence on the electrical performance of b-Si solar cells [10]. As shown in Figure 4, the surface doping concentration of b-Si wafer was reduced from 9.6×10^{20} cm^{-3} to 7.8×10^{20} cm^{-3} via thermal oxidation process, which was due to the further diffusion of the n dopant at temperature of 850°C. When the surface doping concentration at the surface of b-Si wafer was reduced via fabricating SiO_2, the Auger recombination and surface recombination were suppressed, leading to the better electrical performance of S2 cell.

To verify the above presumed further diffusion mechanism, the IQE properties of b-Si with various passivation films were measured, as shown in Figure 5. The IQE of S2 cell is higher than the S1 cell. Compared with the S2 cell, the IQE of S3 cell is higher at 500–900 nm regions, which leads to higher conversion efficiency and I_{sc}. As is well known, in heavily doped silicon, dislocation and dangling bonds are generated due to the mismatch between the covalent radius of an impurity atom occupying substitutional site and the silicon atom, which leads to serving SRH recombination in diffused emitter [16]. The improvement of the IQE and electrical

performances is attributed to the excellent hydrogen passivation, which suppress the SRH recombination near the surface of diffused emitter. In the process of SiN_x:H deposition by PECVD, a large number of hydrogen atoms were generated in SiN_x:H film, which can migrate into silicon to form the Si-H bonds after a thermal treatment, decrease the surface defect state density, and suppress the SRH recombination effectively [17–20]. In the process of metal electrode alloying the silicon wafer temperature is close to 800°C; this process performs the role of thermal treatment [18]. Nevertheless, the IQE between 350–500 nm of the S3 cell is slightly lower than that of S2 cell, which can be explained as follows: (1) the surface state density at Si-SiO_2 interfaces is much lower than that of Si-SiN_x interfaces [17], which leads to the lower surface recombination velocity of S2 cell; (2) the surface doping concentration of S2 is reduced by thermal oxidation process which leads to the suppressing Auger recombination. The S4 cell exhibits the highest IQE at broad band of wavelength which may be assigned to the more effective passivation of SiO_2/SiN_x:H stacks film. Therefore, the short (350–500 nm) and long (500–1100 nm) wave responses were improved by the SiO_2 and SiN_x:H in SiO_2/SiN_x:H stacks film, respectively.

4. Conclusions

In summary, we demonstrated that the conversion efficiency of the large area b-Si solar cells is significantly enhanced by inducing various surface passivation films. The b-Si with binary structure textured surface was produced by silver-nanoparticle-assisted etching, and the length of nanowire is about 250 nm with the R_{ave} of 3.42%. The efficiency of b-Si solar cell without passivation is 13.8%, and the b-Si solar cells with SiO_2, SiN_x:H, and SiO_2/SiN_x:H stacks films increase to 16.1%, 16.5%, and 17.1%, respectively. The b-Si solar cells with SiO_2/SiN_x:H stacks films yield the best electrical performance, and the passivation mechanism can be given as follows: (1) the SiO_2 film not only has low surface state density at Si-SiO_2 interfaces but also reduces the surface doping concentration via thermal oxidation processing leading to the lower Auger recombination; (2) the SiN_x:H can effectively suppress the SRH recombination in the b-Si solar cell, especially in the emitter, which leads to the higher performance of b-Si solar cells.

Conflict of Interests

The authors declare that there is no conflict of interests regarding the publication of this paper.

Acknowledgment

This work is supported by the National High-tech R&D Program of China (863 Program) under Grant no. 2011AA050516.

References

[1] S. K. Srivastava, D. Kumar, P. K. Singh, M. Kar, V. Kumar, and M. Husain, "Excellent antireflection properties of vertical silicon nanowire arrays," *Solar Energy Materials and Solar Cells*, vol. 94, no. 9, pp. 1506–1511, 2010.

[2] K. Peng, Y. Xu, Y. Wu, Y. Yan, S.-T. Lee, and J. Zhu, "Aligned single-crystalline Si nanowire arrays for photovoltaic applications," *Small*, vol. 1, no. 11, pp. 1062–1067, 2005.

[3] M. Moreno, D. Daineka, and P. Roca i Cabarrocas, "Plasma texturing for silicon solar cells: from pyramids to inverted pyramids-like structures," *Solar Energy Materials and Solar Cells*, vol. 94, no. 5, pp. 733–737, 2010.

[4] Y. Xia, B. Liu, J. Liu, Z. Shen, and C. Li, "A novel method to produce black silicon for solar cells," *Solar Energy*, vol. 85, no. 7, pp. 1574–1578, 2011.

[5] Y. Xia, B. Liu, S. Zhong, and C. Li, "X-ray photoelectron spectroscopic studies of black silicon for solar cell," *Journal of Electron Spectroscopy and Related Phenomena*, vol. 184, no. 11-12, pp. 589–592, 2012.

[6] Y. Cao, A. Liu, H. Li et al., "Fabrication of silicon wafer with ultra low reflectance by chemical etching method," *Applied Surface Science*, vol. 257, no. 17, pp. 7411–7414, 2011.

[7] D. Kumar, S. K. Srivastava, P. K. Singh, M. Husain, and V. Kumar, "Fabrication of silicon nanowire arrays based solar cell with improved performance," *Solar Energy Materials and Solar Cells*, vol. 95, no. 1, pp. 215–218, 2011.

[8] H.-C. Yuan, V. E. Yost, M. R. Page, P. Stradins, D. L. Meier, and H. M. Branz, "Efficient black silicon solar cell with a density-graded nanoporous surface: optical properties, performance limitations, and design rules," *Applied Physics Letters*, vol. 95, no. 12, Article ID 123501, 2009.

[9] M. Y. Shen, C. H. Crouch, J. E. Carey, and E. Mazur, "Femtosecond laser-induced formation of submicrometer spikes on silicon in water," *Applied Physics Letters*, vol. 85, no. 23, pp. 5694–5696, 2004.

[10] J. H. Oh, H. C. Yuan, and H. M. Branz, "An 18.2%-efficient black-silicon solar cell achieved through control of carrier recombination in nanostructures," *Nature Nanotechnology*, vol. 7, no. 11, pp. 743–748, 2012.

[11] F. Toor, H. M. Branz, M. R. Page, K. M. Jones, and H.-C. Yuan, "Multi-scale surface texture to improve blue response of nanoporous black silicon solar cells," *Applied Physics Letters*, vol. 99, no. 10, Article ID 103501, 2011.

[12] W. C. Wang, C. W. Lin, H. J. Chen et al., "Surface passivation of efficient nanotextured black Silicon solar cells using thermal atomic layer deposition," *ACS Applied Materials and Interfaces*, vol. 5, no. 19, pp. 9752–9759, 2013.

[13] X. Li and P. W. Bonn, "Metal-assisted chemical etching in HF/H_2O_2 produces porous silicon," *Applied Physics Letters*, vol. 77, no. 16, pp. 2572–2574, 2000.

[14] P. Menna, G. Di Francia, and V. La Ferrara, "Porous silicon in solar cells: a review and a description of its application as an AR coating," *Solar Energy Materials and Solar Cells*, vol. 37, no. 1, pp. 13–24, 1995.

[15] S. Wang, X. Z. Yu, and H. T. Fan, "Simple lithographic approach for subwavelength structure antireflection," *Applied Physics Letters*, vol. 91, no. 6, Article ID 061105, 2007.

[16] X. X. Lin, X. Hua, Z. G. Huang et al., "Realization of high performance silicon nanowire based solar cells with large size," *Nanotechnology*, vol. 24, no. 23, Article ID 235402, 2013.

[17] A. G. Aberle, "Surface passivation of crystalline silicon solar cells: a review," *Progress in Photovoltaics Research and Applications*, vol. 8, no. 5, pp. 473–487, 2000.

[18] F. Duerinckx and J. Szlufcik, "Defect passivation of industrial multicrystalline solar cells based on PECVD silicon nitride," *Solar Energy Materials and Solar Cells*, vol. 72, no. 1–4, pp. 231–246, 2002.

[19] M. Stavola, S. Kleekajai, L. Wen et al., "IR characterization of hydrogen in crystalline silicon solar cells," *Physica B*, vol. 404, no. 23-24, pp. 5066–5070, 2009.

[20] F. Jiang, M. Stavola, A. Rohatgi et al., "Hydrogenation of Si from $SiN_x(H)$ films: characterization of H introduced into the Si," *Applied Physics Letters*, vol. 83, no. 5, pp. 931–933, 2003.